

A ~700 years perspective on the 21st century drying in the eastern part of Europe based on $\delta^{18}\text{O}$ in tree ring cellulose

Viorica Nagavciuc ^{1,2}, Monica Ionita ^{1,2}✉, Zoltán Kern ^{3,4}, Danny McCarroll⁵ & Ionel Popa ^{6,7}

Numerical simulations indicate that extreme climate events (e.g., droughts, floods, heat waves) will increase in a warming world, putting enormous pressure on society and political decision-makers. To provide a long-term perspective on the variability of these extreme events, here we use a ~700 years tree-ring oxygen isotope chronology from Eastern Europe, in combination with paleo-reanalysis data, to show that the summer drying over Eastern Europe observed over the last ~150 years is to the best of our knowledge unprecedented over the last 700 years. This drying is driven by a change in the pressure patterns over Europe, characterized by a shift from zonal to a wavier flow around 1850_{CE}, leading to extreme summer droughts and aridification. To our knowledge, this is the first and longest reconstruction of drought variability, based on stable oxygen isotopes in the tree-ring cellulose, for Eastern Europe, helping to fill a gap in the spatial coverage of paleoclimate reconstructions.

¹ Forest Biometrics Laboratory – Faculty of Forestry, “Stefan cel Mare” University of Suceava, Suceava, Romania. ² Alfred Wegener Institute for Polar and Marine Research, Am Handelshafen Street No. 12, Bremerhaven 27570, Germany. ³ Institute for Geological and Geochemical Research, Research Centre for Astronomy and Earth Sciences, Eötvös Loránd Research Network, Budapest, Hungary. ⁴ CSFK, MTA Centre of Excellence, Konkoly Thege Miklós út 15-17, Budapest H-1121, Hungary. ⁵ Department of Geography, Swansea University, Singleton Park, Swansea SA2 8PP, UK. ⁶ National Research and Development Institute for Silviculture “Marin Drăcea”, Calea Bucovinei no. 76bis, Câmpulung Moldovenesc 725100, Romania. ⁷ INCE—Mountain Economy Center CEMONT, Vatra Dornei, Romania. ✉email: Monica.Ionita@awi.de

The impacts of climate change on society are most strongly felt through the increasing intensity and frequency of extreme events (e.g., floods, drought, heat waves, and/or cold spells)^{1–12}. The economic losses caused by weather- and climate-related events in Europe increased from 7.4 billion Euro in the 1980s to 13 billion Euro over the period 2010–2017¹³. During the 2003 European heatwave ~70,000 heat-related deaths were recorded¹⁴ and >17 billion Euro of direct economic losses were incurred¹³. Climate projections indicate that the frequency and magnitude of extreme events are expected to increase in a warming world¹⁵, but assessing projections against observational data is hampered by the relatively short instrumental records available. In particular, trends based on short records are very sensitive to the beginning and end dates and do not, in general, reflect long-term climate trend¹⁶. Natural paleoclimate archives (e.g., corals, ice cores, shells, sediment records) have become an important tool to supplement instrumental records and tree rings are one of the most valuable¹⁷, due to their annual resolution, precise dating, and widespread occurrence. Tree ring chronologies can be thousands of years long and allow past climate to be explored using a range of paleoclimate proxies, such as tree ring width, maximum density, and stable isotopic composition of the wood or its components^{18,19}. Stable oxygen isotopes have the advantage that the processes of fractionation are well understood and they can record paleoclimate information in areas where other tree-rings proxies do not register the climate signal^{20–23}. Many dendroclimatological studies focused on reconstructing pre-defined teleconnection indices like the North Atlantic Oscillation²⁴, El Niño-Southern Oscillation²⁵, Atlantic Multidecadal Oscillation²⁶ or on the reconstruction of regional temperature and/or precipitation^{27,28}. So far, relatively few studies have tried to link tree-ring-derived proxy signals to synoptic-scale pressure patterns^{21,23,29,30}. However, it is the large-scale atmospheric circulation, through its prevailing high- and low-pressure systems, that strongly controls the frequency and magnitude of extreme events.

This study aims to develop the first annually-resolved tree ring $\delta^{18}\text{O}$ time series for the Eastern Carpathians (Călimani Mountains), Romania (Fig. 1), in order to reconstruct the variability of the summer Standardized Precipitation-Evapotranspiration Index (SPEI) for the last ~700 years and to analyze the link between $\delta^{18}\text{O}$ variability and large-scale atmospheric circulation. The palaeoclimate potential of stable isotopes in *Pinus cembra* L. (Swiss stone pine) tree-ring cellulose from the Călimani Mountains has been demonstrated recently³⁰, showing that $\delta^{18}\text{O}$ variability allows high-resolution paleoclimatic reconstructions over the eastern part of Europe, where few such reconstructions are available.

Results and discussion

Present-day climate. It has been long recognized that persistent high-pressure systems play an important role in the generation of heat waves, soil moisture deficit, and droughts both at global and regional scales^{10,31–34}, and those long-lasting blocking situations associated with stationary Rossby waves are the leading drivers of droughts and heat waves^{1,35–37}. To optimally analyze the link between summer large-scale atmospheric circulation and drought variability at the European level, over the observational record, we computed the coupled modes of variability between summer geopotential height at 500 mb (Z500)³⁸ and August SPEI3 index, by employing a canonical correlation analysis (CCA). The first 10 empirical orthogonal functions (EOF) of Z500 summer (JJA) capture ~80% of the total variance, while the first 10 EOFs of August SPEI3 capture ~85% of the total variance. The optimal number of retained EOFs was chosen so that by adding or

removing one EOF, the CCA would not change considerably³⁹. The first coupled mode of variability between Z500 and SPEI3 reveals that a high-pressure system extending over south, central, and eastern Europe (Fig. 2a) corresponds with drought episodes over the same region (Fig. 2b), and a low-pressure system over the northern Atlantic and northern Europe is correlated with wet climatic conditions over northern Europe. The year-to-year variations of the normalized temporal components of the first CCA pairs are shown in Fig. 2c. The two time-series are significantly correlated ($r = -0.91$, $p < 0.01$). The negative correlations between standardized amplitudes corresponding to CCA1 Z500 and CCA1 August SPEI3 (Fig. 2c) confirm the significant relationship between drought variability at the European scale and large-scale atmospheric circulation. The two canonical time series present strong interannual variability, over the 1901–2015CE period, with the highest amplitudes (towards higher pressure and drought) over the 21st century. Overall, dry (wet) periods over the analyzed region are driven by the occurrence of a high (low) pressure system extending over most of the European continent and a low (high) pressure system over Iceland extending up to Fennoscandia.

$\delta^{18}\text{O}$ Chronology description. A stable oxygen isotope chronology, spanning 1331–2012CE, was constructed by measuring $\delta^{18}\text{O}$ on the cellulose of individual tree rings using 16 trees (five living trees and eleven dead wood samples) (Fig. 3a and Supplementary Figure 1). The shortest and longest analyzed sections contained 90 and 370 tree rings, respectively (Table 1). Replication varies between two and five trees, with a two-replication record between 1331 and 1372CE, and the highest replication for the 20th century, while for most of the chronology the replication is four (Fig. 3). The mean of the $\delta^{18}\text{O}$ raw values is 28.8‰ and the data ranges between 26.7‰ in 1837CE and 31.6‰ in 1946CE. The $\delta^{18}\text{O}$ chronology presents periods with low $\delta^{18}\text{O}$ values: 1428–1466, 1644–1703, 1800–1823, and 1967–1988, and periods with high $\delta^{18}\text{O}$ values: 1470–1487, 1621–1636, 1704–1720, 1890–1962, and 1989–2012. Subsample Signal Strength (SSS) varies between 0.85 and 0.95 for the analyzed period, while the mean inter-series correlation (R_{bar}) and the Expressed Population Signal (EPS) values for the 1331–2012CE period range between 0.51 and 0.93, and between 0.80 and 0.98, respectively, for different time windows (Fig. 3), indicating that a strong common signal is preserved^{40,41}. The linear reconstruction model ($r = -0.71$, $p < 0.001$) is thus strong and temporally stable, passing all of the conventional verification tests (Supplementary Figure 2).

The $\delta^{18}\text{O}$ values of tree-ring cellulose are mainly affected by the isotopic ratio of precipitation, which varies in response to the atmospheric pressure patterns during the summer⁴². Further fractionation occurs in the leaf, driven mainly by the difference between internal and external water vapor pressures, and thus by relative humidity¹⁹. Dry summer conditions thus lead to higher $\delta^{18}\text{O}$ values in leaf sugars and therefore wood cellulose, so that, a negative correlation between tree ring $\delta^{18}\text{O}$ and the SPEI index is expected.

Climate reconstruction. The reconstruction of August SPEI, for an accumulation period of 3 months (SPEI3) (Supplementary Figure 2), extends back to 1331CE (Fig. 4a). Variations of the $\delta^{18}\text{O}$ values capture the August SPEI3 changes both at high and low frequencies (from interannual to multidecadal scales). For the reconstructed period, 44 years of extremely low and 45 years of extremely high SPEI3 values were found (Table 2, Supplementary Tables 1 and 2). However, their temporal distribution is not uniform over time, and several distinct periods can be

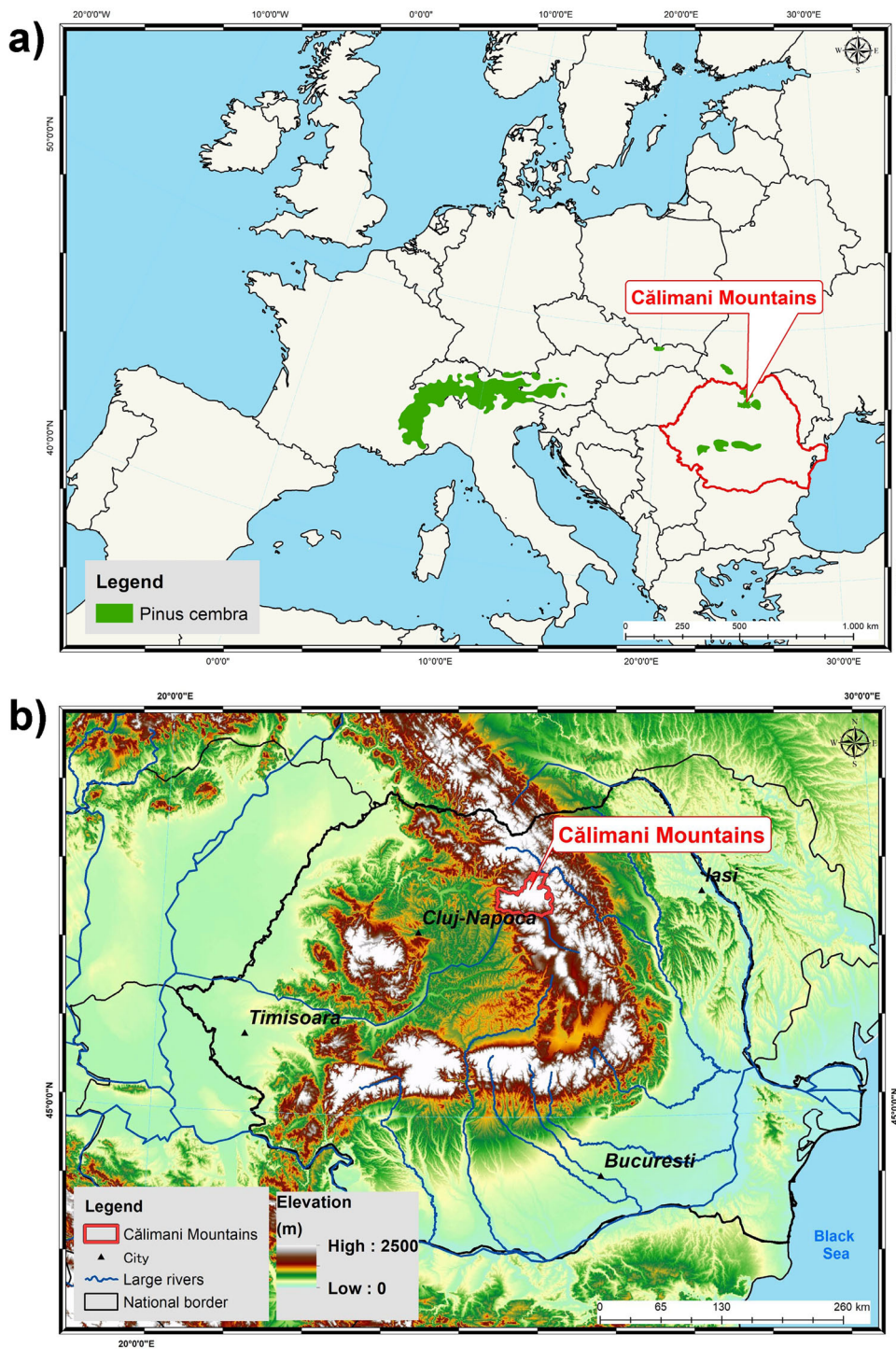


Fig. 1 Location of the investigation area. **a** Distribution of *Pinus cembra* in Europe⁹⁹, and **b** topographic map of Romania showing the sampling site.

highlighted. The period 1331–1500CE is characterized by nine low extreme years, and seven high extreme years. The period between 1500 and 1850CE is characterized by predominantly high extreme years (33 years from a total of 45) and only 18 low extreme years. After 1850CE low extreme years dominate (17 negative extreme years from 44, and only five high extreme years). The last high extreme year was recorded in 1955CE, while over the 1990–2012CE period were recorded 7 extreme low years. The temporal distribution of the extreme years overlaps very well with the frequency of extreme events from other regions of

Europe. The high frequency of the positive extreme events during the 1500–1850CE period overlaps with the Little Ice Age, characterized by reoccurring cold and wet climatic conditions in this region^{43,44}. In contrast, the only three positive extreme events and a higher frequency of negative extremes in the most recent part of the chronology could be related to the global climate change signal^{15,16}. Our reconstruction indicates that the 20th and early 21st centuries are unprecedented, in terms of dryness, since 1331CE (Fig. 4b). The extreme events reported here correspond with historical reports of catastrophic events (Supplementary

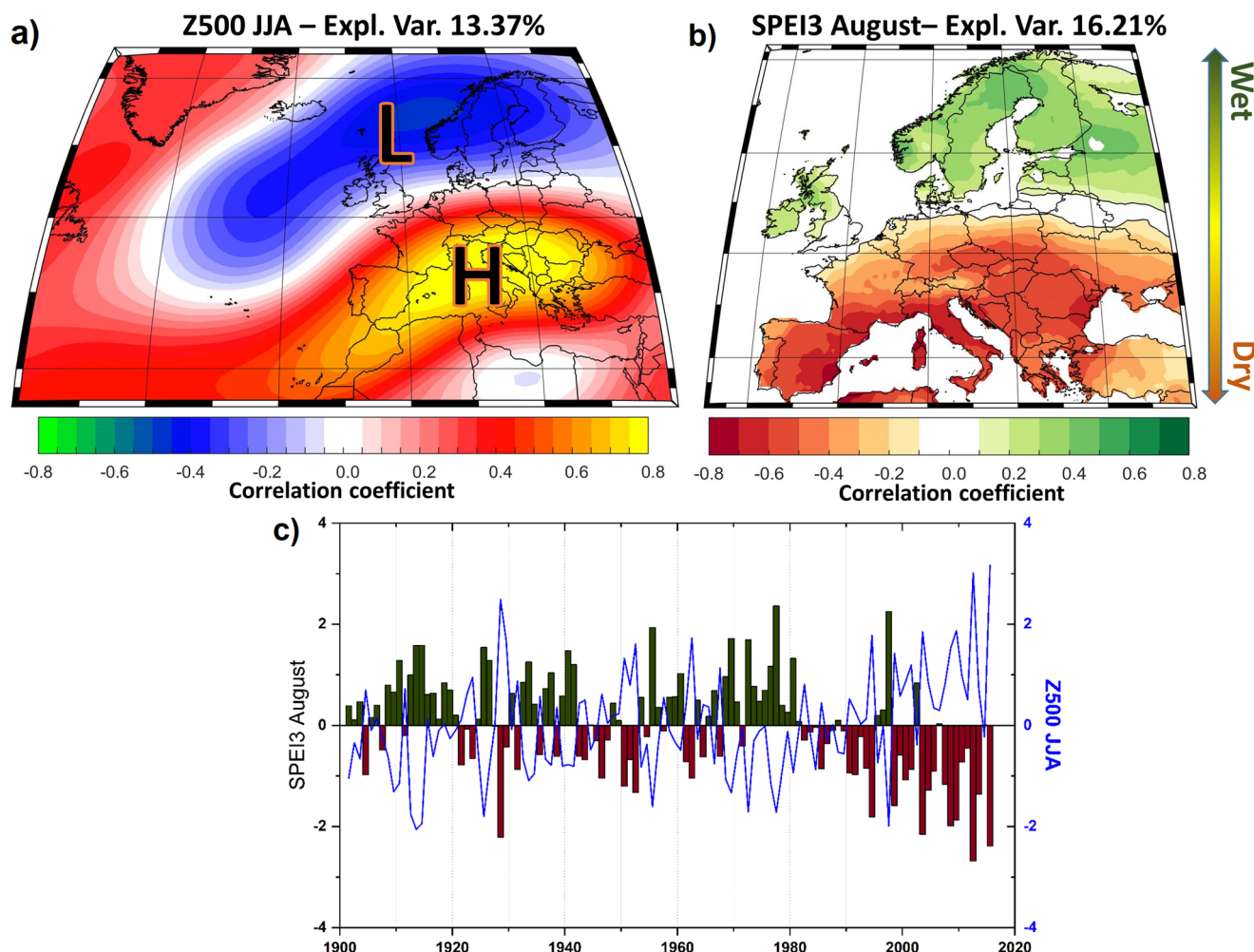


Fig. 2 Coupled modes of variability. The first coupled mode of variability (CCA1) between **a** summer Z500 and **b** August SPEI3; **c** the standardized amplitudes corresponding to CCA1-Z500 (blue line) and CCA1-SPEI3 (bars).

Tables 1 and 2). For example, the 1585CE drought is known as a very dry year, especially in spring, over the analyzed region. During the summer months, all the springs and pools dried and trees were killed by drought^{45,46}. The year 1904, a negative extreme according to our reconstruction, was characterized by an extended drought in Moldova⁴⁷. In Romania, it was so dry that the government had to take measures to avoid famine⁴⁶. The 1904CE drought persisted for 18 months (from June 1903_{CE} until the end of 1904CE). This year was reported as a dry year also in Switzerland and France⁴⁵. The year 1946CE was one of the most severe droughts recorded in the 20th century and was characterized by very warm and dry conditions, with many absolute maximum temperature values greater than +40 °C in Moldova and Romania^{45–47}. Historical sources have been used to analyze also positive extremes (wet years). For instance, 1593CE had a wet spring and summer, with a lot of rainfall and continuous floods^{46,47}, not only in Romania but also in Ukraine⁴⁵. In 1684CE catastrophic floods were reported over the analyzed region⁴⁷, mainly due to four weeks of constant rain⁴⁵. The year with the highest amplitude in our reconstruction is 1816CE, known as the “year without a summer”, with heavy rains, linked to the climatic aftermath of the eruption of Tambora^{45,48}. Therefore, the robustness of our August SPEI3 reconstruction is validated by the good match of extreme years recorded by our reconstruction with historical sources for the last ~700 years (Supplementary Tables 1 and 2).

The large-scale atmospheric circulation in a long-term context.

Based on spatial correlation/stability maps, it appears that the spatial correlation pattern between $\delta^{18}\text{O}$ values and SPEI3 over the last 110 years is stable in time and shows a clear dipole-like structure with negative and significant correlations over the central, southeast, and eastern parts of Europe, and positive and significant correlations over the northern and north-western parts of Europe³⁰. Nagavciuc et al. (2020)³⁰ have shown that during summer, high $\delta^{18}\text{O}$ values in Swiss stone pine tree rings in the Călimani Mountains are associated with dry conditions over central, southeast, and eastern Europe, while low $\delta^{18}\text{O}$ values are associated with wet summers over the eastern part of Europe. The dry and warm climatic conditions increase the contrast between ambient and intercellular vapor pressures, increasing the fractionation of oxygen isotopes in the foliage which transferred to the synthesized cellulose and archived in tree rings^{20,49}, as well as changing the isotope ratios in precipitation. Overall, the strong correlation obtained for August SPEI3, explains 50.4% of local drought variability over the eastern part of Europe. Although the strong relationship between $\delta^{18}\text{O}$ variability in tree rings from the eastern part of Europe, and large-scale atmospheric circulation has been reported^{21,30}, this relationship was analyzed only over the observational record, covering the 20th century. In order to examine how large-scale atmospheric circulation can explain long-term drought variability, we computed composite maps using summer northern hemisphere geopotential height at

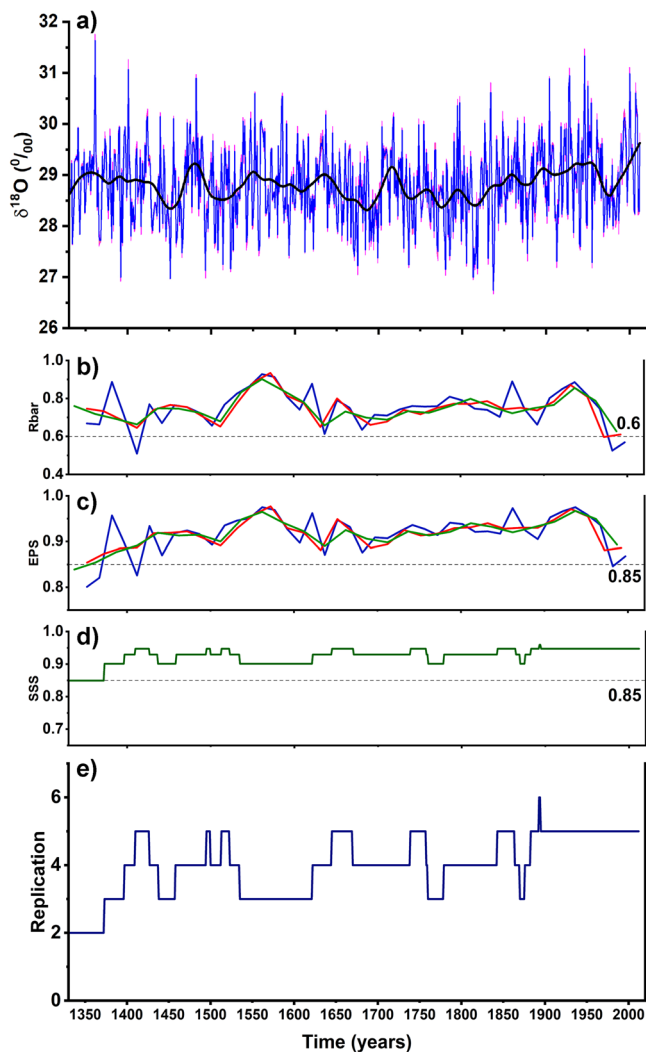


Fig. 3 Raw $\delta^{18}\text{O}$ values and the corresponding statistics. **a** The raw $\delta^{18}\text{O}$ values measured in the *Pinus cembra* L. from Călimani Mountains, Romania (blue line), 31-year running mean (black line), and 95% calculated confidence level of the raw $\delta^{18}\text{O}$ values (pink line). **b** The inter-series correlation (Rbar) values calculated for the raw $\delta^{18}\text{O}$ series with different running window: 50 years with an overlap of 25 years (green line), 40 years with 20 years overlap (red line), and 30 years with 15 years overlap (blue line). **c** The Expressed Population Signal (EPS) calculated with different running window: 50 years with an overlap of 25 years (green line), 40 years with 20 years overlap (red line), and 30 years with 15 years overlap (blue line). **d** Subsample Signal Strength (SSS) for the raw $\delta^{18}\text{O}$ series (green line). **e** Replication (dark blue line). The gray bars represent time periods for which the replication is ≤ 2 .

500 mb (Z500) from the 20th century reanalysis data over the period 1836–2012CE (Supplementary Figure 3) as well as by using paleoclimate reanalysis data⁵⁰ for the period 1604–2003CE (Fig. 5). The composite map analyses based on both datasets show similar results. Wet years (SPEI3 values $> +1$ standard deviation) are associated with a low-pressure center over the central and eastern part of Europe and a high-pressure system over the northern Atlantic Ocean and northern Europe (Fig. 5a), while the dry years (SPEI3 values < -1 standard deviation) are associated with a high-pressure center over the central and eastern part of Europe and a low-pressure system over the northern Atlantic Ocean and northern Europe (Fig. 5b). These results are in

agreement with the results reported by Nagavciuc et al. (2020)³⁰. During summer, the low-pressure center over the central and eastern part of Europe is associated with a cyclonic circulation, which facilitates the advection of moist air from the Mediterranean region towards Romania, leading to above normal precipitation over this region (Fig. 5a)^{35,51}. The high-pressure center over the central and eastern parts of Europe is associated with anticyclonic circulation, which favors the advection of dry and warm air from the northern part of Africa toward the southeastern part of Europe thus generating very dry and hot summers over the study site (Fig. 5b).

Stability of the drought signal in the reconstruction. The relationship between large-scale atmospheric circulation and European climate has been found to be non-stationary in time, especially when pre-defined teleconnection indices are used^{32,52,53}. In order to overcome the problem of non-stationarity and to test if the identified relationship between the reconstructed SPEI3 index and the large-scale atmospheric circulation is stable over time, we employed a methodology used for the monthly to seasonal prediction of the mean runoff of the Elbe River^{51,54}, but also applied in dendroclimatological studies^{30,55}. Over the last 400 years the relationship between the reconstructed SPEI3 index and summer (JJA) Z500 is stable, showing a significant negative correlation over a large part of eastern Europe (Supplementary Figure 4). Based on the stability map (Supplementary Figure 4), we have defined a Z500 index averaged over the central and eastern part of Europe (black square in Supplementary Figure 4) to place the evolution of the increased high pressure over this region in a long-term context (Fig. 6). Over the last 400 years, prolonged dry (wet) years were associated with positive (negative) Z500 anomalies over the central and eastern parts of Europe. Although until 1850CE, both time series show no significant change in their temporal evolution, starting with ~1850 both time series present a significant (99% significance level) negative (SPEI3) and positive (Z500) trend. The 31-year running mean of the SPEI3 intersects with summer Z500 around 1860 CE, after which their opposing trends continue until the present (Fig. 6c). From a statistical perspective⁵⁶, the year 1860 CE appears as a change point in both time series (Fig. 6c). The values of SPEI3 and summer Z500 index are both unprecedented over the 20th and 21st centuries. The box plot of August SPEI3 index and Z500 index over two distinct periods 1604–1850 and 1851–2002 CE (Supplementary Figure 5) indicates that there is a significant difference ($p \ll 0.001$, based on a two-test sample, Kolmogorov and Smirnov) in the distribution of the two-time series over these two time periods. The 1604–1850 CE period is characterized by a higher frequency of wet years and lower Z500 values, while the period 1851–2002 CE is characterized by an increase in dry years and a shift towards higher values of the Z500 index. A similar abrupt shift in the values of $\delta^{18}\text{O}$, at ~1850 CE, has been captured in a coral record from the northern Red Sea⁵⁷. The shift in the $\delta^{18}\text{O}$ coral record was interpreted as being driven by a reorganization of the large-scale atmospheric circulation, which is in agreement with our findings. Moreover, at a decadal time scale (e.g., after applying a running mean of 31 years) the tree-ring $\delta^{18}\text{O}$ record correlates with the coral $\delta^{18}\text{O}$ time series from the northern Red Sea at the 99% significance level ($r = -0.80$).

To further emphasize the influence of Z500 anomalies on the variability of the reconstructed August SPEI3, we also computed the changes in the occurrence of concurrent extremes (e.g., positive Z500 anomalies/low SPEI3) over the last 400 years. Throughout the analyzed period, drought events were accompanied by positive Z500 anomalies, with an increased frequency after 1850 CE (Fig. 6d).

Table 1 The analyzed trees and tree ring chronology length.

Tree name	Type	TRW chronology length	Analyzed period	Study
Tree 1	Living	1871-2012	1876-2012	(Nagavciuc et al.) ³⁰
Tree 2	Living	1888-2012	1893-2012	(Nagavciuc et al.) ³⁰
Tree 3	Living	1878-2012	1883-2012	(Nagavciuc et al.) ³⁰
Tree 4	Living	1724-2012	1876-2012	(Nagavciuc et al.) ³⁰
			1739-1875	This study
Tree 5	Living	1770-2012	1843-2012	This study
Tree 6	Subfossil	1766-1894	1779-1894	This study
Tree 7	Subfossil	1621-1869	1645-1869	This study
Tree 8	Subfossil	1485-1864	1495-1864	This study
Tree 9	Subfossil	1620-1759	1622-1759	This study
Tree 10	Subfossil	1513-1790	1513-1757	This study
Tree 11	Subfossil	1373-1534	1373-1534	This study
Tree 12	Subfossil	1270-1695	1331-1522	This study
Tree 13	Subfossil	1410-1499	1410-1499	This study
Tree 14	Subfossil	1204-1789	1251-1436	This study
Tree 15	Subfossil	1441-1775	1459-1670	This study
Tree 16	Subfossil	1008-1426	1397-1426	This study

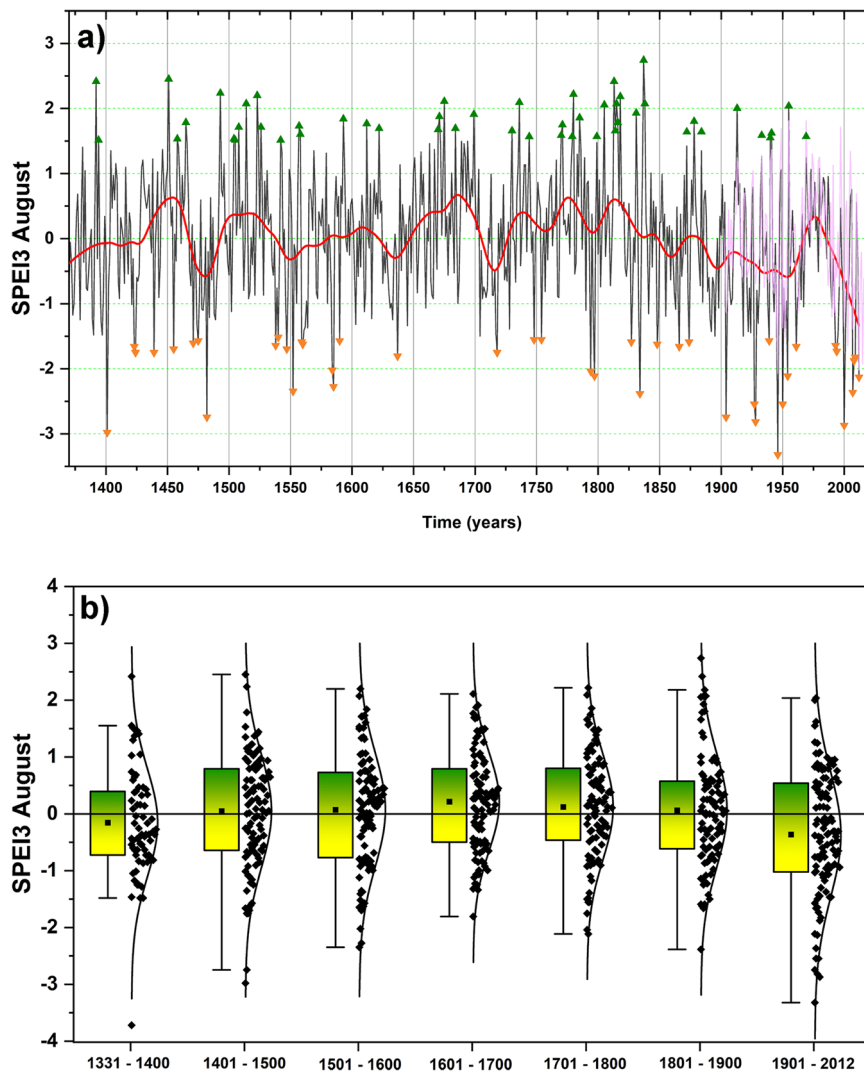


Fig. 4 Drought index reconstruction. **a** Reconstructed August SPEI3 (black line) for 1331-2012CE period, with the 31-year running mean (red line) and measured August SPEI3 for 1902-2012CE period (magenta line). Extreme dry/wet years are represented as lower-orange/upper-green triangles. Extreme years are defined when the SPEI3 index is lower than -1.5 or higher than $+1.5$ standard deviation. **b** Box plots of the reconstructed August SPEI3 for different centuries over the period 1331 (1301)-2012CE.

Table 2 The years corresponding to the low values (August SPEI3 < -1.5) and high values (August SPEI3 > 1.5) over the 1331-2012CE period.

Years with extreme low values	Years with extreme high values
1361, 1401, 1423, 1424, 1439, 1455, 1471, 1475, 1482, 1538, 1540, 1547, 1552, 1559, 1560, 1584, 1585, 1590, 1637, 1718, 1748, 1754, 1794, 1797, 1827, 1834, 1848, 1866, 1874, 1904, 1927, 1928, 1939, 1946, 1950, 1954, 1961, 1993, 1994, 2000, 2007, 2008, 2009, 2012	1334, 1392, 1451, 1458, 1465, 1493, 1504, 1505, 1508, 1514, 1523, 1526, 1542, 1557, 1558, 1593, 1612, 1622, 1670, 1671, 1675, 1684, 1694, 1699, 1736, 1740, 1770, 1771, 1675, 1684, 1699, 1730, 1736, 1744, 1770, 1771, 1780, 1785, 1805, 1813, 1814, 1815, 1816, 1818, 1831, 1837, 1838, 1878, 1913, 1940, 1941, 1955

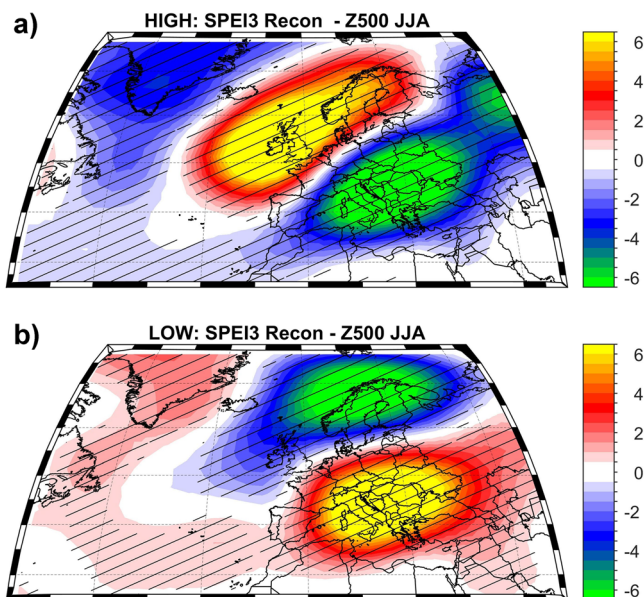


Fig. 5 Large-scale atmospheric circulation. **a** The composite map between High SPEI3 (< -1 std. dev.) and summer (JJA) Geopotential Height at 500 mb (Z500)¹⁰⁰ and **b** the composite map between Low SPEI3 (>1 std. dev.) and summer (JJA) Geopotential Height at 500 mb (Z500). The hatching highlights significant anomalies at a confidence level of 95%. Units: Z500 (m). Analyzed period: 1604-2003CE.

Drought at European scale. To have a long-term perspective of our reconstruction in comparison with other hydroclimatic reconstructions available at European scale and to assess their spatial synchronicity, our reconstructed August SPEI3 time series was compared with other reconstructions available at European scale. In a first step we compared our August SPEI3 time-series with the Old World Drought Atlas (OWDA)⁵⁸ averaged over the region 25°E-28°E, 46°N-48°N (Supplementary Figure 6). As it can be inferred from Supplementary Figure 6 there are important differences of variability and magnitude between our reconstructions and the OWDA-based time-series. Overall, the OWDA does not capture low-frequency drought variability and does not show any trend over the 20th and 21st centuries (Supplementary Figure 6). The mean values of the OWDA reconstruction are below 0 for the whole analyzed period, with the minimum (driest) during the 17th century and the maximum during the 20th century. In contrast, our August SPEI3 reconstruction, based on stable isotope data that has not been statistically de-trended, retains low-frequency variability, with the maximum August SPEI3 values (wet) during the 17th century and with the minimum in the 20th century, results that are in a good agreement with the historical evidence and more recent observations (Supplementary Tables 1 and 2). Our results emphasize that paleoclimate reconstructions focused on the western and northern parts of Europe cannot explain the complex spatial variability of

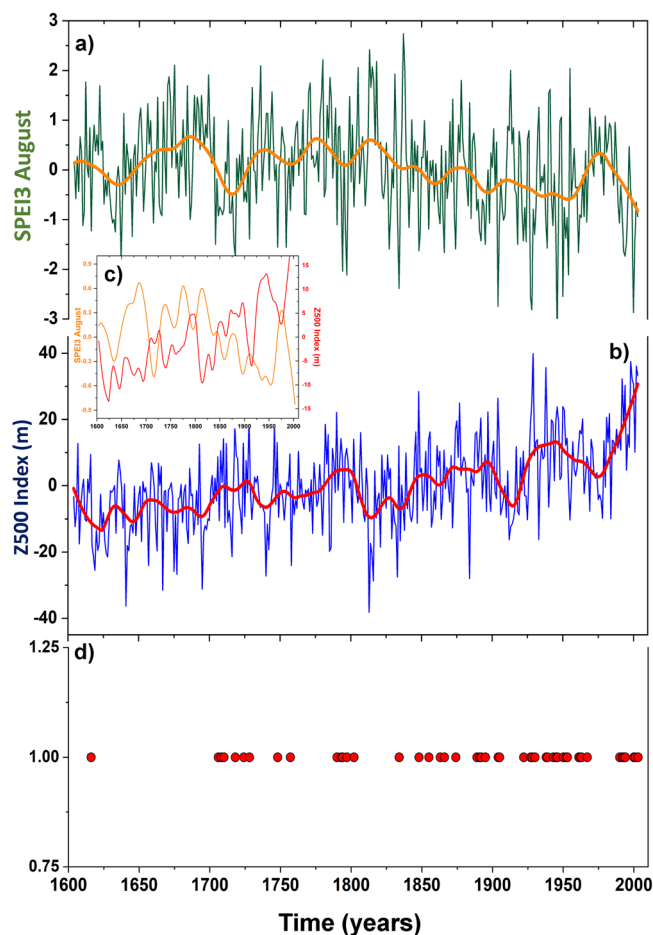


Fig. 6 Drought reconstruction and large-scale drivers. **a** Reconstructed SPEI 3 (green line) and 31-year running mean (orange line); **b** summer (JJA) Z500 time series averaged over the stable region: 13.5°E-35.0°E, 30°N-52°N (blue line) and 31-year running mean (red line). **c** The direct comparison between the 31-year running mean for SPEI 3 reconstruction (orange line) and for summer Z500 time series (red line) and **d** Occurrence of positive Z500 anomalies and dry events (Z500₇₅/SPEI3₂₅). Z500₇₅/SPEI3₂₅ indicates that we took into account the common years when the Z500 anomalies were higher than the 75th percentile and SPEI3 was smaller than the 25th percentile.

climate over the entire continent, especially over the eastern part of Europe. For example, the recent reconstruction based on tree-rings stable isotopes from the Czech Republic and Southern Germany⁵⁹, only shows strong correlations over a small region of central Europe (Fig. 3b in their paper). The strong offset between our reconstruction and the Büntgen et al. (2021)⁵⁹ drought reconstruction (Supplementary Figure 7) emphasizes the need for an extended network of reconstructions covering the entire Europe. Overall, it is clear from Supplementary Figure 7 that the

drought reconstruction from a small region like the Czech Republic and southern Germany are not able to capture fully the drought variability at European scale. This is further emphasized by comparing our reconstruction to drought history from the Czech Republic and southern Germany⁵⁹, and a drought reconstruction covering the entire Germany⁶⁰. Although the two reconstructions^{59,60} are coming from closely related regions, even over some overlapping ones (such as southern Germany), wet (dry) periods over Germany as recorded by August SPEI3⁶⁰ are not matching with wet (dry) periods as recorded by the drought reconstruction from the Czech Republic and southern Germany (Supplementary Figure 7b and 7c). Similar results have been recently shown by Ionita et al. (2021)³⁶, which have shown that the recent droughts of 2015 and 2018 are not unprecedented over the central part of Europe (with a focus on Germany), which is in disagreement with the conclusions of Büntgen et al. (2021)⁵⁹ study and in agreement with the findings of Glaser and Kahle (2020)⁶⁰. Therefore, a priority for a better understanding of climatic variability over Europe is high-resolution paleoclimate reconstructions in the Eastern part of Europe and not only.

Comparisons of our summer drought reconstruction and other reconstructions across Europe (Fig. 7 and Supplementary Figure 8) indicates the August SPEI3 is in agreement with reconstructions preserving similar characteristic of the spatial variability. The Călimani August SPEI3 record accords with the summer temperature reconstruction for the same site⁶¹ and with summer (JJA) SPEI reconstruction over France⁶² (Fig. 7). The lack of low-frequency variability in the other precipitation and drought reconstructions based on tree-ring width from the vicinity of the study area precludes a direct comparison with our August SPEI3 reconstruction, therefore we also computed the 31 years running mean for each reconstruction (Supplementary Figure 8i, j, k, l, m, n, o, p). Overall, the results showed that our reconstruction retains both high and low-frequency variability similar to other reconstructions; however, their synchronicity is not stable in time. The high-frequency similarities are expressed through the extreme years registered by different reconstructions. On a decadal time scale, our August SPEI3 record accords with reconstructions from the North Aegean⁶³, Czech Republic^{64–66}, southwestern Turkey⁶⁷, Eastern Mediterranean⁶⁸, and from the south-eastern part of Romania⁶⁹ (Supplementary Figure 8). Decadal-scale variability of extreme climatic conditions also appears robust. For example, the 1470–1490CE period represents one of the most severe drought periods, recognized in numerous studies over Europe^{70,71}. The drought conditions in this period were severe across Europe and can also be observed in the OWDA drought reconstruction (Fig. 7). This period is also characterized by high-temperature anomalies in the study area, as well as over the central part of Europe (Fig. 7). Another example of the severe long-term drought condition prevailed from 1700 to 1730CE is in the opposite phase with the drought conditions over Scandinavia⁷², emphasizing the dipole-like structure in the drought conditions over Europe⁷³. This dipole structure is even more obvious in the last decades when southern and central-eastern Europe show an increase in the drought severity and frequency, while the SPEI reconstructions for northern and western Europe show a tendency towards wetter conditions. This dipole structure can be also seen when looking at wet periods in the reconstructed SPEI3 indices (Fig. 7). For example, the 1585–1615CE and 1800–1830CE periods are characterized by wet climatic conditions and high-temperature anomalies over southern central, and eastern Europe, while over the northern part of Europe dry conditions prevailed.

Conclusions. In this study, we report the first reconstruction of the summer (June to August) Standardized Precipitation-

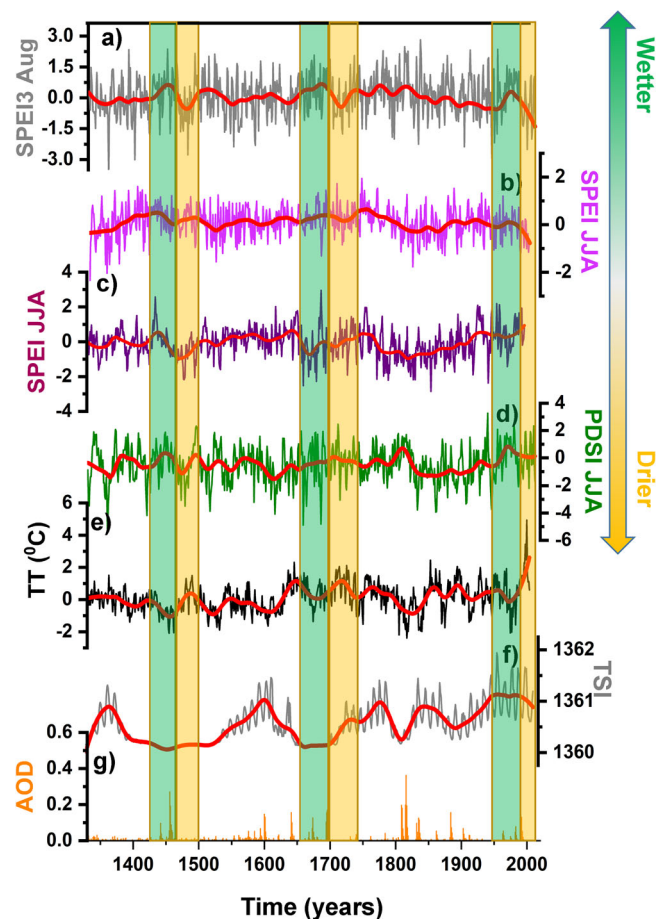


Fig. 7 Comparison among different reconstructions at European level.

a Reconstructed August SPEI3 based on the $\delta^{18}\text{O}$ in tree ring cellulose from Călimani Mts. from 1331 to 2012 period (gray line). **b** Summer (JJA) SPEI reconstruction over France (magenta line)⁶² over the period 1326–2004CE. **c** Summer (JJA) SPEI2 reconstruction over Scandinavia (green line)⁷² for the period 1272–1995CE. **d** Regional mean Old World Drought Atlas (OWDA) drought index averaged over the eastern part of Europe (25°E–28°E, 46°N–48°N, green line) for the period 1252–2012CE⁵⁸. **e** Summer temperature reconstruction over Romania (black line)⁶¹. **f** Time series of annual total solar irradiance (light gray)¹⁰¹ and **g** Aerosol optical depth (AOD, orange bars)¹⁰². The bold red lines in (a–f) represent the 31 years running mean for each time series.

Evapotranspiration Index (SPEI3), 1331–2012CE, for eastern Europe, based on annually-resolved stable oxygen isotope ratios ($\delta^{18}\text{O}$) from *Pinus cembra* L. tree-ring cellulose from the Călimani Mountains, Romania. Variation of $\delta^{18}\text{O}$ captures the SPEI3 changes at both high and low frequencies, revealing changes in the prevailing large-scale atmospheric circulation over central Europe. At the end of the Little Ice Age (~1850CE), there was a shift in the large-scale atmospheric circulation towards higher pressure systems over the central and eastern parts of Europe, which led to a drying tendency over the eastern part of Europe over the 20th and 21st centuries, which to the best of our knowledge is unprecedented over the last ~700 years (Fig. 2b). This is the first and longest reconstruction of drought variability for eastern Europe based on stable oxygen isotopes in tree-ring cellulose, helping to fill a missing gap in the spatial coverage of paleoclimate reconstructions.

Methods

Study site and local climate. The Călimani Mountains belong to a volcanic chain, situated in the north-western part of the central Eastern Carpathians (Fig. 1). With

the highest peaks exceeding 2000 m, the region experiences a mountain temperate-continental climate, with severely cold winters and cool summers. The mean maximum annual temperature over the analyzed region is 8.5 °C and ranges between -2.7 °C in January and +18.8 °C in July–August⁷⁴. Mean annual precipitation is 889 mm, with a summer peak in June–July when amount exceeds 100 mm/month⁷⁴. During winter, thick snow cover can last for up to 200 days. Forests are dominated by Swiss stone pine (*Pinus cembra* L.) mixed with Norway spruce (*Picea abies* Karst., L.) which are replaced by mountain pine (*Pinus mugo*) towards higher elevations. Since 1975 the area has been protected due to natural forests with old trees and abundant subfossil wood. Open-pit sulfur mining was operated nearby between 1965 and 1992CE, with the most intense activity during 1974–1986CE⁷⁵ disturbing the climate-growth relationship and leaving clear signals also in the chemical composition of the wood⁷⁶.

Sample collection, preparation, and stable isotope measurements. The Swiss stone pine samples were collected in autumn of 2012, from Călimani Mountains (Călimani National Park) (Fig. 1), from elevations ranging from 1450 m a.s.l. to 1850 m a.s.l. (treeline) while the current timberline is situated at 1700 m a.s.l.⁷⁷. In total, 16 cores (one core per tree) were used for stable isotopic measurements, out of which five were living trees (labeled Tree 1 to 5) and eleven were subfossil trees (labeled Tree 6 to 16). From the living trees, samples were collected using an 11 mm diameter increment borer, while for the subfossil trunks found on the forest floor, a sample disk was sawn, and the trunks were left in the original place. Tree-ring widths (TRW) of samples were measured using LINTAB equipment and TSAP 0.53 software, with 0.001 mm accuracy for accurate cross-dating against the local master chronology⁶¹ and checked for missing rings or dating accuracy with COFECHA software⁷⁸. The analyses of stable oxygen isotopes were performed for the 1331–2012CE period (Fig. 3). The tree ring samples were split with a scalpel to obtain annual resolution before measurement of each ring individually (no pooling). Alpha-cellulose, extracted using the modified Jayme-Wise method^{79,80}, was homogenized by a standard ultrasonic protocol⁸¹ using VCX130 (Sonic & Materials Inc/USA) device and dried at 70 °C for 24 h. For the measurements of oxygen isotope ratios ($\delta^{18}\text{O}$), 0.2 mg ($\pm 10\%$) of α -cellulose was packed in silver foil and pyrolyzed over glassy carbon at 1450 °C using a ThermoQuest TCEA interfaced with a Thermo Delta V Advantage IRMS^{82,83}. All isotope values are reported in per mil (‰) relative to the Vienna Standard Mean Ocean Water (VSMOW)⁸⁴, using the traditional δ (delta) notation. The analytical precision of the measurements was better than 0.1‰. All samples were measured in triplicates, but if their standard deviation exceeded 0.2‰ two additional measurements were performed to check potential outliers and reduce uncertainty. The individual $\delta^{18}\text{O}$ series were tested systematically for trend effect during the juvenile years in a separate study^{30,85}. Since they do not show any age trend, the raw $\delta^{18}\text{O}$ can be used for further paleoclimatic reconstruction. In order to minimize any effect of offset between individual time series, the method described by the Nakatsuka et al. (2020)⁸⁶, was applied to combine the individual time series into a composite $\delta^{18}\text{O}$ chronology. The Expressed Population Signal (EPS) and the inter-series correlation (Rbar) values were calculated for the $\delta^{18}\text{O}$ series for the 1331–2012CE period, with different running windows: 50 years with an overlap of 25 years, 40 years with 20 years overlap, and 30 years with 15 years overlap. Also, Subsample Signal Strength (SSS) was calculated for the same period. We do not combine oxygen and carbon isotope results because the mechanistic controls on fractionation are different¹⁹ and they do not carry the same climate signal²⁹.

Climate data and statistical methods. The potential of climate signals in oxygen isotope ratios of Swiss stone pine tree-ring cellulose from the Călimani Mountains was tested in a separate paper³⁰. According to the results reported³⁰, the highest correlation coefficients and best statistical skill were obtained for $\delta^{18}\text{O}$ values and relative humidity at the local scale, and $\delta^{18}\text{O}$ and the summer SPEI drought index at the European scale. The correlation between $\delta^{18}\text{O}$ chronology and the SPEI index was tested for different months and different periods of accumulation (from one month to 12 months), and the highest coefficient of correlation was obtained for SPEI3 August (Supplementary Figure 9). As such, the SPEI3 August drought index was used to provide a long record of summer drought conditions over the eastern part of Europe. For the reconstruction model we used the Standardized Precipitation Evapotranspiration Index (SPEI) covering 1902–2012CE. SPEI was computed based on the monthly precipitation (PP), monthly mean air temperature (TT), and the potential evapotranspiration (PET) data from the CRU T.S. 4.04 dataset⁷⁴ dataset using the R-package SPEI (<https://cran.r-project.org/web/packages/SPEI/index.html>) and has a spatial resolution of $0.5^\circ \times 0.5^\circ$.

Calibration and verification procedure. The reconstruction model of the drought index was developed using the R packages *dplR*⁸⁷ and *treeclim*⁸⁸, using the linear regression method. To test the predictive skills of the model for drought index reconstruction, the data were split into two equal periods: calibration and verification (Supplementary Figure 2). The reduction of error (RE), coefficient of efficiency (CE), and R^2 statistics were used to assess the skill of the regression model⁸⁹. The Durbin–Watson statistic (DW) was used to test the trend in the residuals⁹⁰. The calibration and verification models passed all of the conventional verification tests, both in the forward and the reverse modes. For the August SPEI3

model, the RE = 0.63, CE = 0.63 and DW = 1.82 for the forward model, and RE = 0.43, CE = 0.42 and DW = 1.83 for the reverse model. The positive values of the RE and CE indicate good predictive skills of the model, which suggest that the reconstruction model is robust and stable over time. The DW test values indicate that the residuals of the SPEI3 model have low autocorrelation. The results of the statistical tests indicate that the reconstruction model was reliable and can be considered for the reconstruction of August SPEI3 at local and at the European scale. When a linear regression model is used for climate reconstruction, the variance underestimates that of the target data^{91,92}, so the reconstructed August SPEI3 values were rescaled with mean zero and one standard deviation.

Canonical correlation analysis (CCA). To identify the coupled patterns of variability between the summer large-scale atmospheric circulation (Z500) and August SPEI3, we used a Canonical Correlation Analysis (CCA). CCA is a powerful multivariate technique used to identify pairs of patterns with the maximum correlation between their associated time series³⁹. Before applying a CCA, the dimensionality of August SPEI3 and geopotential height at 500 mb (Z500) datasets were reduced by an Empirical Orthogonal Function (EOF) analysis. The first 10 EOFs of JJA Z500 and August SPEI3 were retained as input in the CCA. The first 10 EOFs of Z500 JJA capture ~80% of the total variance, while the first 10 EOFs of August SPEI3 capture ~85% of the total variance. The optimal number of retained EOFs was chosen in such a way that by adding or removing one EOF, the CCA would not change considerably³⁹. Among other statistical methods, CCA has the advantage of selecting pairs of optimally correlated spatial patterns, which may lead to a physical interpretation of the mechanism controlling the climate variability.

Stability maps. To test the stability of the relationship between the reconstructed drought index and the summer geopotential height, we make use of stability maps, a methodology successfully used in the seasonal forecast of the European rivers and Antarctic sea ice to examine the stationarity of the long-term relationship between our proxies and the gridded climate data^{54,93,94}. In order to detect stable predictors, the variability of the correlation between the tree-ring parameters and the gridded data is investigated within a 51-year moving window over the 1604–2003CE period. The correlation is considered stable for those regions where the tree-ring parameter and the gridded data are significantly correlated at the 90 or 80% level for more than 80% of the moving window. The basic idea of this methodology is to identify regions with stable correlations (meaning the correlation does not change over time) between August SPEI3 and summer Z500.

Compound events. To test the influence of Z500 on the probability of occurrence of dry events, we employ a joint frequency analysis of compound events⁹⁵ (e.g., the co-occurrence of positive Z500 anomalies and dry events)⁹⁶. For each time series (e.g., Z500 and SPEI3 August) we computed a binary variable ($Y = 1$ for co-occurrence and $Y = 0$ for non-occurrence) which indicates the occurrence based on Z500 and SPEI3. For the specific threshold of the variables, the occurrence of a compound event can be expressed as:

$$Y = \begin{cases} 1, & P \leq px, T > tx \\ 0, & \text{otherwise} \end{cases} \quad (1)$$

where px indicates the precipitation threshold and tx indicates the temperature threshold, for example. For the current analysis, we have chosen as threshold the 75th percentile for Z500 and the 25th percentile for SPEI3 August.

Sources of uncertainty. Paleoclimatic reconstructions give us the opportunity to explore climatic variability from times for which we do not have measured data, but every reconstruction contains a range of uncertainties. The sources of uncertainty are numerous and can occur at every step of the process⁹⁷. The use of wood samples from the same site removed uncertainties arising from different wood sources or possible differences in the registered signal. Measuring the isotope ratio on individual rings, rather than pooling⁹⁸, and measuring at least three times, although expensive, ensures high precision, necessarily balanced by low replication. The reconstruction is based on three to five tree replications, and only for the period 1331–1373CE the replication is only two (Fig. 3). The potential offset between individual time series was removed by using the method described by Nakatsuka et al. (2020)⁸⁶, to combine the individual time series into a composite chronology. The statistical properties of the composite chronology are good and the absence of any statistical de-trending ensures that it is possible to retain climatic information at all frequencies. In summary, our approach favors precision over replication, so the main source of uncertainty lies in the limited replication. The chronology provides, however, a firm foundation to which more data can be added in the future, allowing the magnitude of uncertainty to be both reduced and quantified more precisely.

Data availability

The reconstructed August SPEI3 index can be downloaded from here: <https://doi.org/10.5281/zenodo.7243885> (Nagavciuc et al., 2022).

Received: 26 January 2021; Accepted: 27 October 2022;

Published online: 15 November 2022

References

- Della-Marta, P. M. et al. Summer heat waves over western Europe 1880–2003, their relationship to large-scale forcings and predictability. *Clim. Dyn.* **29**, 251–275 (2007).
- Meehl, G. A. & Tebaldi, C. More intense, more frequent, and longer lasting heat waves in the 21st century. *Science* **305**, 994–997 (2004).
- Twardosz, R. & Kossowska-Cezak, U. Exceptionally hot summers in Central and Eastern Europe (1951–2010). *Theor. Appl. Climatol.* **112**, 617–628 (2013).
- Beniston, M. & Stephenson, D. B. Extreme climatic events and their evolution under changing climatic conditions. *Glob. Planet. Change* **44**, 1–9 (2004).
- Rebetez, M. et al. Heat and drought 2003 in Europe: a climate synthesis. *Ann. For. Sci.* **63**, 569–577 (2006).
- Barriopedro, D., Fischer, E. M., Luterbacher, J., Trigo, R. M. & García-Herrera, R. The hot summer of 2010: map of Europe. *Science* **332**, 220–224 (2011).
- Dole, R. et al. Was there a basis for anticipating the 2010 Russian heat wave? *Geophys. Res. Lett.* **38**, 1–5 (2011).
- Bissolli, P. et al. Drought conditions in Europe in the spring of 2012. *DWD - Deutscher Wetterdienst* 1–30, https://www.dwd.de/EN/ourservices/specialevents/drought/20120810_Trockenheit_2012_en.html (2012).
- Carrington, D. 2012: the year Britain's weather turned dangerous. *The Guardian* 1, <https://www.theguardian.com/environment/2013/jan/04/2012-year-british-weather-dangerous> (2012).
- Ionita, M. et al. The European 2015 drought from a climatological perspective. *Hydrol. Earth Syst. Sci.* **21**, 1397–1419 (2017).
- Ionita, M. & Nagavciuc, V. Forecasting low flow conditions months in advance through teleconnection patterns, with a special focus on summer 2018. *Sci. Rep.* **10**, 13258 (2020).
- Coumou, D. & Rahmstorf, S. A decade of weather extremes. *Nat. Clim. Chang.* **2**, 491–496 (2012).
- European Union. European Union, Economic losses from climate related extremes in Europe (<https://www.eea.europa.eu/data-and-maps/indicators/direct-losses-from-weather-disasters-3/assessment-2>) (2018).
- Robine, J. M. et al. Death toll exceeded 70,000 in Europe during the summer of 2003. *Comptes Rendus - Biol* **331**, 171–178 (2008).
- IPCC. *Global warming of 1.5 °C An IPCC Special Report on the Impacts of Global Warming of 1.5 °C above Pre-industrial Levels and Related Global Greenhouse Gas Emission Pathways, in the Context of Strengthening the Global Response to the Threat of Climate Change.* https://www.ipcc.ch/site/assets/uploads/sites/2/2018/07/SR15_SPM_High_Res.pdf (2018).
- IPCC. *IPCC Climate Change 2014 Synthesis Report. Contribution of Working Groups I, II and III to the Fifth Assessment Report of the Intergovernmental Panel on Climate Change* (eds. Core Writing Team, Pachauri, R. K. and Meyer, L. A.) (IPCC, 2014).
- Jones, P. D. et al. High-resolution palaeoclimatology of the last millennium: A review of current status and future prospects. *Holocene* **19**, 3–49 (2009).
- Hughes, M. K., Swetnam, T. W. & Diaz, H. F. *Dendroclimatology Progress and Prospects.* <https://doi.org/10.1007/978-1-4020-5725-0> (Springer, 2011).
- Cook, B. I. et al. Megadroughts in the Common Era and the Anthropocene. *Nat. Rev. Earth Environ.* <https://doi.org/10.1038/s43017-022-00329-1> (2022).
- McCarroll, D. & Loader, N. J. Stable isotopes in tree rings. *Quat. Sci. Rev.* **23**, 771–801 (2004).
- Nagavciuc, V. et al. Stable oxygen isotopes in Romanian oak tree rings record summer droughts and associated large-scale circulation patterns over Europe. *Clim. Dyn.* **52**, 6557–6568 (2019).
- Young, G. H. F. et al. Oxygen stable isotope ratios from British oak tree-rings provide a strong and consistent record of past changes in summer rainfall. *Clim. Dyn.* **45**, 3609–3622 (2015).
- Andreu-Hayles, L. et al. 400 Years of summer hydroclimate from stable isotopes in Iberian trees. *Clim. Dyn.* **49**, 143–161 (2017).
- Trouet, V., Babst, F. & Meko, M. Recent enhanced high-summer North Atlantic Jet variability emerges from three-century context. *Nat. Commun.* **9**, 1–9 (2018).
- D'Arrigo, R., Cook, E. R., Wilson, R. J., Allan, R. & Mann, M. E. On the variability of ENSO over the past six centuries. *Geophys. Res. Lett.* **32**, 1–4 (2005).
- Gray, S. T., Graumlich, L. J., Betancourt, J. L. & Pederson, G. T. A tree-ring based reconstruction of the Atlantic Multidecadal Oscillation since 1567 A.D. *Geophys. Res. Lett.* **31**, 2–5 (2004).
- Esper, J. et al. Large-scale, millennial-length temperature reconstructions from tree-rings. *Dendrochronologia* **50**, 81–90 (2018).
- Loader, N. J. et al. Summer precipitation for the England and Wales region, 1201–2000 CE, from stable oxygen isotopes in oak tree rings. *J. Quat. Sci.* **35**, 731–736 (2020).
- Zhang, P., Ionita, M., Lohmann, G., Chen, D. & Linderholm, H. W. Can tree-ring density data reflect summer temperature extremes and associated circulation patterns over Fennoscandia? *Clim. Dyn.* **49**, 2721–2736 (2017).
- Nagavciuc, V. et al. Climate signals in carbon and oxygen isotope ratios of Pinus cembra tree-ring cellulose from Călimani Mountains, Romania. *Int. J. Climatol.* **40**, 2539–2556 (2020).
- Swain, D. L., Horton, D. E., Singh, D. & Diffenbaugh, N. S. Trends in atmospheric patterns conducive to seasonal precipitation and temperature extremes in California. *Sci. Adv.* **2**, 1–14 (2016).
- Ionita, M., Rimbu, N. & Lohmann, G. Decadal variability of the Elbe River streamflow. *Int. J. Climatol.* <https://doi.org/10.1002/joc.2054> (2011).
- Schubert, S. D., Wang, H., Koster, R. D., Suarez, M. J. & Groisman, P. Y. Northern Eurasian heat waves and droughts. *J. Clim.* **27**, 3169–3207 (2014).
- Kingston, D. G., Stagge, J. H., Tallaksen, L. M. & Hannah, D. M. European-scale drought: understanding connections between atmospheric circulation and meteorological drought indices. *J. Clim.* **28**, 505–516 (2015).
- Ionita, M., Lohmann, G., Rimbu, N., Chelcea, S. & Dima, M. Interannual to decadal summer drought variability over Europe and its relationship to global sea surface temperature. *Clim. Dyn.* **38**, 363–377 (2012).
- Ionita, M., Dima, M., Nagavciuc, V., Scholz, P. & Lohmann, G. Past megadroughts in central Europe were longer, more severe and less warm than modern droughts. *Commun. Earth Environ.* **2**, 61 (2021).
- Ionita, M., Nagavciuc, V., Kumar, R. & Rakovec, O. On the curious case of the recent decade, mid-spring precipitation deficit in central Europe. *npj Clim. Atmos. Sci.* **3**, 49 (2020).
- Slivinski, L. C. et al. Towards a more reliable historical reanalysis: Improvements for version 3 of the Twentieth Century Reanalysis system. *Q. J. R. Meteorol. Soc.* **145**, 2876–2908 (2019).
- von Storch, H. & Zwiers, F. W. *Statistical Analysis in Climate Research.* <https://doi.org/10.1017/cbo9780511612336> (Cambridge University Press, 1999).
- Wigley, T. M. L., Briffa, K. R. & Jones, P. D. On the average value of correlated time series, with applications in dendroclimatology and hydrometeorology. *J. Clim. Appl. Meteorol.* **23**, 201–213 (1984).
- Buras, A. A comment on the expressed population signal. *Dendrochronologia* **44**, 130–132 (2017).
- Gagen, M. et al. in *Stable Isotopes in Tree Rings. Tree Physiology* (eds. Siegwolf, R. T. W., Brooks, J. R., Roden, J. & Saurer, M.) 537–579 (Springer International Publishing, 2022).
- Kern, Z. et al. Natural proxy records of temperature- and hydroclimate variability with annual resolution from the Northern Balkan–Carpathian region for the past millennium – Review & recalibration. *Quat. Int.* **415**, 109–125 (2016).
- Perşoiu, A. in *Landform Dynamics and Evolution in Romania* (eds. Radoane, M. & Vespremeanu-Stroe, A.) 57–66 (Springer International Publishing, 2017).
- Teodoreanu, E. *În căutarea timpului trecut Schiță de climatologie istorică* (Editura Paodeia, 2017).
- Topor, N. *Anii ploioși și secetoși din Republica Populară Română* (C.S.A Institutul Meteorologic, 1963).
- Mihăilescu, C. *Clima și hazardurile Moldovei: evoluția, starea, predicția* (Licorn, 2004).
- Esper, J., Schneider, L., Krusic, P. J., Sirocko, F. & Zorita, E. European summer temperature response to annually dated volcanic eruptions over the past nine centuries. *Bull. Volcanol.* **75**, 736 (2013).
- Roden, J., Lin, G. & Ehleringer, J. R. A mechanistic model for interpretation of hydrogen and oxygen isotope ratios in tree-ring cellulose. *Geochim. Cosmochim. Acta* **64**, 21–35 (2000).
- Franke, J. G., Werner, J. P. & Donner, R. V. Reconstructing Late Holocene North Atlantic atmospheric circulation changes using functional paleoclimate networks, supplementary material. *Supplement to: Franke, J. G. et al. (2017): Reconstructing Late Holocene North Atlantic atmospheric circulation changes using functional paleoclimate networks. Climate of the Past, 13(11), 1593–1608, https://doi.org/10.5194/cp-13-1593-2017* (2017).
- Ionita, M. Interannual summer streamflow variability over Romania and its connection to large-scale atmospheric circulation. *Int. J. Climatol.* **35**, 4186–4196 (2015).
- Walter, K. & Graf, H. F. On the changing nature of the regional connection between the North Atlantic Oscillation and sea surface temperature. *J. Geophys. Res. Atmos.* **107**, ACL 7–1–ACL 7-13 (2002).
- Lu, J. & Greatbatch, R. J. The changing relationship between the NAO and northern hemisphere climate variability. *Geophys. Res. Lett.* **29**, 52-1–52-4 (2002).
- Ionita, M., Lohmann, G. & Rimbu, N. Prediction of spring Elbe discharge Based on stable teleconnections with winter global temperature and precipitation. *J. Clim.* **21**, 6215–6226 (2008).
- Nagavciuc, V. et al. Different climate response of three tree ring proxies of Pinus sylvestris from the Eastern Carpathians, Romania. *Dendrochronologia* **54**, 56–63 (2019).

56. Worsley, K. J. On the likelihood ratio test for a shift in location of normal populations. *J. Am. Stat. Assoc.* **74**, 365–367 (1979).
57. Felis, T., Ionita, M., Rimbu, N., Lohmann, G. & Kölling, M. Mild and arid climate in the Eastern Sahara-Arabian Desert during the Late Little Ice Age. *Geophys. Res. Lett.* **45**, 7112–7119 (2018).
58. Cook, E. R. et al. Old World megadroughts and pluvials during the Common Era. *Sci. Adv.* **e1500561** 6, 1–10 (2015).
59. Büntgen, U. et al. Recent European drought extremes beyond Common Era background variability. *Nat. Geosci.* **14**, 190–196 (2021).
60. Glaser, R. & Kahle, M. Reconstructions of droughts in Germany since 1500—combining hermeneutic information and instrumental records in historical and modern perspectives. *Clim. Past* **16**, 1207–1222 (2020).
61. Poppo, I. & Kern, Z. Long-term summer temperature reconstruction inferred from tree ring records from the Eastern Carpathians. *Clim. Dyn.* **32**, 1107–1117 (2009).
62. Labuhn, I. et al. French summer droughts since 1326 CE: a reconstruction based on tree ring cellulose $\delta^{18}\text{O}$. *Clim. Past* **12**, 1101–1117 (2016).
63. Griggs, C., DeGaetano, A., Kuniholm, P. & Newton, M. A regional high-frequency reconstruction of May–June precipitation in the north Aegean from oak tree rings, A.D. 1089–1989. *Int. J. Climatol.* **27**, 1075–1089 (2007).
64. Dobrovolný, P. et al. May–July precipitation reconstruction from oak tree-rings for Bohemia (Czech Republic) since AD 1040. *Int. J. Climatol.* **38**, 1910–1924 (2018).
65. Brázdil, R. et al. Documentary and instrumental-based drought indices for the Czech Lands back to AD 1501. *Clim. Res.* **70**, 103–117 (2016).
66. Brázdil, R., Štepanková, P., Kyncl, T. & Kyncl, J. Fir tree-ring reconstruction of March–July precipitation in southern Moravia (Czech Republic), 1376–1996. *Clim. Res.* **20**, 223–239 (2002).
67. Touchan, R. et al. Preliminary reconstructions of spring precipitation in Southwestern Turkey from tree-ring width. *Int. J. Climatol.* **23**, 157–171 (2003).
68. Touchan, R. et al. Reconstructions of spring/summer precipitation for the Eastern Mediterranean from tree-ring widths and its connection to large-scale atmospheric circulation. *Clim. Dyn.* **25**, 75–98 (2005).
69. Levančić, T., Popa, I., Poljansek, S. & Nechita, C. A 323-year long reconstruction of drought for SW Romania based on black pine (*Pinus nigra*) tree-ring widths. *Int. J. Biometeorol.* **57**, 703–714 (2013).
70. Pribyl, K. & Cornes, R. C. Droughts in medieval and early modern England, part 1: the evidence. *Weather* **75**, 168–172 (2020).
71. Camenisch, C. et al. Extreme heat and drought in 1473 and their impacts in Europe in the context of the early 1470s. *Reg. Environ. Chang.* **20**:19, 1–15 (2020).
72. Seftigen, K., Goosse, H., Klein, F. & Chen, D. Hydroclimate variability in Scandinavia over the last millennium—insights from a climate model-proxy data comparison. *Clim. Past* **13**, 1831–1850 (2017).
73. Ionita, M., Boroneanț, C. & Chelcea, S. Seasonal modes of dryness and wetness variability over Europe and their connections with large scale atmospheric circulation and global sea surface temperature. *Clim. Dyn.* **45**, 2803–2829 (2015).
74. Harris, I., Osborn, T. J., Jones, P. & Lister, D. Version 4 of the CRU TS monthly high-resolution gridded multivariate climate dataset. *Sci. Data* **7**, 1–18 (2020).
75. Brânduș, C. & Cristea, I. Anthropogenic impact in the Călimani’s caldera. *Analele Univ. Vest din Timișoara, Geogr.* **XIV**, 159–168 (2004).
76. Kern, Z., Popa, I., Varga, Z. & Széles, É. Degraded temperature sensitivity of a stone pine chronology explained by dendrochemical evidences. *Dendrochronologia* **27**, 121–128 (2009).
77. Kern, Z. & Popa, I. Changes of frost damage and treeline advance for Swiss Stone Pine in the Calimani Mts. (Eastern Carpathians, Romania). *Acta Silv. Lignaria Hungarica* **4**, 39–48 (2008).
78. Holmes, R. L. Computer-assisted quality control in tree-ring dating and measurement. *Tree Ring Bull* **43**, 69–75 (1983).
79. Boettger, T. et al. Wood cellulose preparation methods and mass spectrometric analyses of $\delta^{13}\text{C}$, $\delta^{18}\text{O}$, and nonexchangeable $\delta^2\text{H}$ values in cellulose, sugar, and starch: an interlaboratory comparison. *Anal. Chem.* **79**, 4603–4612 (2007).
80. Loader, N. J., Robertson, I., Barker, A. C., Switsur, V. R. & Waterhouse, J. S. An improved technique for the batch processing of small wholewood samples to α -cellulose. *Chem. Geol.* **136**, 313–317 (1997).
81. Laumer, W. et al. A novel approach for the homogenization of cellulose to use micro-amounts for stable isotope analyses. *Rapid Commun. Mass Spectrom* **23**, 1934–1940 (2009).
82. Saurer, M., Robertson, I., Siegwolf, R. & Leuenberger, M. Oxygen isotope analysis of cellulose: an interlaboratory comparison. *Anal. Chem.* **70**, 2074–2080 (1998).
83. Leuenberger, M. C. & Filot, M. S. Temperature dependencies of high-temperature reduction on conversion products and their isotopic signatures. *Rapid Commun. Mass Spectrom* **21**, 1587–1598 (2007).
84. Coplen, T. B. Reporting of stable hydrogen, carbon, and oxygen isotopic abundances. *Pure Appl. Chem* **66**, 273–276 (1994).
85. Kern, Z., Nagavciuc, V., Hatvani, I. G., Loader, N. J. & Popa, I. Evaluation of the age related systematic patterns of stable oxygen and carbon isotope values of Swiss stone pine (*Pinus cembra* L.) Eastern Carpathians, Romania. *Dendrochronologia - under Rev.* **DENDRO-S-22-00142**, 1–22 (2022).
86. Nakatsuka, T. et al. A 2600-year summer climate reconstruction in central Japan by integrating tree-ring stable oxygen and hydrogen isotopes. *Clim. Past* **16**, 2153–2172 (2020).
87. Bunn, A. G. A dendrochronology program library in R (dplR). *Dendrochronologia* **26**, 115–124 (2008).
88. Zang, C. & Biondi, F. Treeclim: an R package for the numerical calibration of proxy-climate relationships. *Ecography* **38**, 431–436 (2015).
89. Cook, E. R., Briffa, K. R. & Jones, P. D. Spatial regression methods in dendroclimatology: a review and comparison of two techniques. *Int. J. Climatol.* **14**, 379–402 (1994).
90. Durbin, J. & Watson, G. S. Testing for serial correlation in least squares regression: I. *Biometrika* **37**, 409–428 (1950).
91. Esper, J., Frank, D., Wilson, R. & Briffa, K. R. Effect of scaling and regression on reconstructed temperature amplitude for the past millennium. *Geophys. Res. Lett.* **32**, L07711 (2005).
92. McCarroll, D., Young, G. H. F. & Loader, N. J. Measuring the skill of variance-scaled climate reconstructions and a test for the capture of extremes. *Holocene* **25**, 618–626 (2015).
93. Ionita, M., Dima, M., Lohmann, G., Scholz, P. & Rimbu, N. Predicting the June 2013 European flooding based on precipitation, soil moisture, and sea level pressure. *J. Hydrometeorol* **16**, 598–614 (2014).
94. Ionita, M., Scholz, P., Grosfeld, K. & Treffeisen, R. Moisture transport and Antarctic sea ice: Austral spring 2016 event. *Earth Syst. Dyn.* **9**, 939–954 (2018).
95. Hao, M. et al. Contribution of atmospheric moisture transport to winter Arctic warming. *Int. J. Climatol.* **39**, 2697–2710 (2019).
96. Hao, Z., Hao, F., Xia, Y., Singh, V. P. & Zhang, X. A monitoring and prediction system for compound dry and hot events. *Environ. Res. Lett.* **14**, 114034 (2019).
97. Carré, M., Sachs, J. P., Wallace, J. M. & Favier, C. Exploring errors in paleoclimate proxy reconstructions using Monte Carlo simulations: Paleotemperature from mollusk and coral geochemistry. *Clim. Past* **8**, 433–450 (2012).
98. Liñán Dorado, I. et al. Pooled versus separate measurements of tree-ring stable isotopes. *Sci. Total Environ.* **409**, 2244–2251 (2011).
99. Ulber, M., Gugerli, F. & Bozic, G. *EUFORGEN Technical Guidelines for Genetic Conservation and Use for Swiss Stone Pine (*Pinus cembra*)* (International Plant Genetic Resources Institute, 2004).
100. Franke, J., Brönnimann, S., Bhend, J. & Brugnara, Y. A monthly global paleo-reanalysis of the atmosphere from 1600 to 2005 for studying past climatic variations. *Sci. Data* **4**, 1–19 (2017).
101. Lean, J. L. Estimating solar irradiance since 850 CE. *Earth Sp. Sci.* **5**, 133–149 (2018).
102. Crowley, T. J. Causes of climate change over the past 1000 years. *Science* **289**, 270–277 (2000).

Acknowledgements

The research leading to these results has received funding from EEA Financial Mechanism 20092014 under the project contract no CLIMFOR18SEE. V.N. was supported partially by the project number PN-III-P1-1.1-PD-2019-0469. M.I. is supported by Helmholtz funding through the joint program “Changing Earth - Sustaining our Future” (PoF IV) program of the AWI. Funding by the AWI Strategy Fund Project - PalEX and by the Helmholtz Climate Initiative - REKLIM is gratefully acknowledged. I.P. was supported partially by the project PN-III-P4-PCE-2021-1002 and CresPerfInst (contract 34PFE/30.12.2021). We acknowledge support by the Open Access Publication Funds of Alfred Wegener Institute Helmholtz Centrum for Polar and Marine Research. We would like to thank Professor Nakatsuka T. for sharing the offset methodology script and to Dr. Schloz P. for helping with technical and programming tasks. Also, we would like to thank the administration of the Călimani National Park for sampling permission and support.

Author contributions

V.N. designed the study and wrote the paper. M.I. analyzed the climate data and helped write the paper and interpret the results. V.N. and Z.K. analyzed the samples. M.I., Z.K., D.M., and I.P. helped write the paper and interpret the results.

Funding

Open Access funding enabled and organized by Projekt DEAL.

Competing interests

The authors declare no competing interests.

Additional information

Supplementary information The online version contains supplementary material available at <https://doi.org/10.1038/s43247-022-00605-4>.

Correspondence and requests for materials should be addressed to Monica Ionita.

Peer review information *Communications Earth & Environment* thanks the anonymous reviewers for their contribution to the peer review of this work. Primary Handling Editors: Regina Rodrigues, Joe Aslin, Heike Langenberg.

Reprints and permission information is available at <http://www.nature.com/reprints>

Publisher's note Springer Nature remains neutral with regard to jurisdictional claims in published maps and institutional affiliations.



Open Access This article is licensed under a Creative Commons Attribution 4.0 International License, which permits use, sharing, adaptation, distribution and reproduction in any medium or format, as long as you give appropriate credit to the original author(s) and the source, provide a link to the Creative Commons license, and indicate if changes were made. The images or other third party material in this article are included in the article's Creative Commons license, unless indicated otherwise in a credit line to the material. If material is not included in the article's Creative Commons license and your intended use is not permitted by statutory regulation or exceeds the permitted use, you will need to obtain permission directly from the copyright holder. To view a copy of this license, visit <http://creativecommons.org/licenses/by/4.0/>.

© The Author(s) 2022